Waste Isolation Pilot Plant

Compliance Certification Application

Reference 120

Chappell, J., and N.J. Shackelton. 1986.
Oxygen Isotopes and Sea Level, Nature. Vol. 324, no. 6093, 137-140.

DATE: 02/28/96
DELIVERY DUE: 03/18/96

WESTINGHOUSE ELECTRIC CORPORATION
WASTE ISOLATION DIVISION
P.O. BOX 2078
CARLSBAD, NM 88221

PURCHASE ORDER PO   72919

PAGE: 1 of 3

VENDOR: 156085
Information Express

2250 Ash St.,
Palo Alto, CA 94306

PAYMENT TERMS: 1% 10 NET 30 DAYS
FOB: Destination Prepaid & Not Allowed
SHIP VIA: UPS GROUND

This Order is issued under Westinghouse Prime Contract
DE-AC04-86AL31950 with the U.S. Dept. of Energy. DPAS no. E2
rating applies.

SHIP TO: Westinghouse Electric Corp.
Waste Isolation Division
For the U.S. Dept. of Energy
WIPP Site
30 Miles Southeast of Carlsbad
Carlsbad, NM 88220

BILL TO: Westinghouse Electric Corp.
Waste Isolation Division
Accounts Payable Dept.
P.O. Box 2078
Carlsbad, NM 88221

NOTE: RECEIVING HOURS - 7:30 A.M. TO 3:00 P.M. MONDAY THRU FRIDAY

SD-RDN/WO Sol? : SB
P.O. Coding : XX12

QA Code : M10
West Commodity : GDR

Acct Commodity : 42

Line Number	Item ID / Description	Quantity Ordered	U/M	Unit Price	U/M	Total Price
1	71510-00123 PUBLICATION, BOOKS, BOOKLETTES, PAMPHLETTS. SEE NOTE FOR SPECS.	10.00000	EA	18.000	EA	180.00

BELL, J.T., D.A. COSTANZO, AND W.E. BIGGERS 1973B
PLUTONIUM POLYMERIZATION -- II
KINETICS OF THE PLUTONIUM POLYMERIZATION
JOURNAL OF INORGANIC AND NUCLEAR CHEMISTRY VOL. 35: 623-628

| 2 | 71510 00123 PUBLICATION, BOOKS, BOOKLETTES, PAMPHLETTS. SEE NOTE FOR SPECS. | 10.00000 | EA | 18.000 | EA | 180.00 |

BELL, J.T., C.F. COLEMAN, D.A. COSTANZO, AND R.E. BIGGERS. 1973A
PLUTONIUM POLYMERIZATION -- III
THE NITRATE PRECIPITATION OF PU (IV) POLYMER
JOURNAL OF INORGANIC AND NUCLEAR CHEMISTRY VOL. 35: 629-632

| 3 | 71510-00123 PUBLICATION, BOOKS, BOOKLETTES, PAMPHLETTS. SEE NOTE FOR SPECS. | 10.00000 | EA | 9.000 | EA | 90.00 |

BREDEHOEFT, J.D., RILEY, F.S., AND ROKLOFFS, E.A. 1987
EARTHQUAKES AND GROUNDWATER
EARTHQUAKES AND VOLCANOS, VOL. 19, NO.4, PP. 138-146

| 4 | 71510-00123 PUBLICATION, BOOKS, BOOKLETTES, PAMPHLETTS. SEE NOTE FOR SPECS. | 10.00000 | EA | 21.000 | EA | 210.00 |

CHAPPELL, J., AND N.J. SHACKELTON 1986
OXYGEN ISOTOPES AND SEA LEVEL
NATURE VOL. 324, NO.6093 137-140
REFERENCE CONTROL NUMBER 95205143547

| 5 | 71510-00123 PUBLICATION, BOOKS, BOOKLETTES, PAMPHLETTS. SEE NOTE FOR SPECS. | 10.00000 | EA | 20.000 | EA | 200.00 |

DAVIES, P.B. 1984
DEEP-SEATED DISSOLUTION AND SUBSIDENCE IN BEDDED SALT DEPOSITS
PH.D. DISSERTATION STANFORD, CA
DEPARTMENT OF APPLIED EARTH SCIENCES
STANFORD UNIVERSITY
PALO ALTO, CA
PUBLISHED IN ENGINEERING GEOLOGY, VOL. 27, #44, 12/89 PG.467

| 6 | 71510-00123 PUBLICATION, BOOKS, BOOKLETTES, PAMPHLETTS. SEE NOTE FOR SPECS. | 10.00000 | EA | 21.000 | EA | 210.00 |

HARTMAN, W.K. 1965
TERRESTRIAL AND LUNAR FLUX OF LARGE METEORITES IN THE LAST
TWO BILLION YEARS
ICARUS VOL. 4, NO.2, PP. 157-165

| 7 | 71510-00123 PUBLICATION, BOOKS, BOOKLETTES, PAMPHLETTS. SEE NOTE FOR SPECS. | 10.00000 | EA | | | 3.00 |

IMAN, R.L., AND W.J. CONOVER. 1982
A DISTRIBUTION-FREE APPROACH TO INDUCING RANK CORRELATION
AMONG INPUT VARIABLES

Continued on Next Page
Acknowledgment Copy

9K5 L 317

XE

NM0200

LETTERSTONATURE

137

Oxygen isotopes and sea level

J. Chappell* & N. J. Shackleton†

* Biogeography and Geomorphology, Research School of Pacific
Studies, Australian National University, Canberra, Australia
† Godwin Laboratory for Quaternary Research, University of
Cambridge, Free School Lane, Cambridge CB2 3RS, UK

From the time that detailed oxygen isotope records derived from
foraminifera living in the constant-temperature environment of
the abyssal ocean became available, there has been a discrepancy
between the ice volume record that these records imply, and that
derived from the altitude of dated coral terraces around the world.
Here, we re-examine the data and conclude that the temperature
of the abyssal ocean has been an actively varying component of
the climate system.

Oxygen isotope ratios in foraminifera from deep-sea sedi-
ments have been used as indicators of past climate following
Emiliani's pioneering work[1]. $\delta^{18}O$ in foraminifera varies with
$\delta^{18}O$ in the water from which their carbonate tests are deposited,
but differs from the water value by an amount that is temperature
dependent[2]. The mean $\delta^{18}O$ of the whole ocean varies with the
quantity of isotopically light ice stored on the continents so that
the record from foraminifera in a particular core is a blend of
global (ice volume) and local (temperature) components. As
the record in planktonic foraminifera may be affected by
differences in surface salinity[3] as well as by changing seasonal
growth and depth habitat[4], benthic foraminifera have recently
been preferred as they provide a less complicated record of
global ice volume. It has been assumed that the deep ocean, at
least in the Pacific, is so cold that its temperature may be
regarded as constant as well as spatially uniform.

Differences exist between $\delta^{18}O$ records from different cores,
even those based on benthic foraminifera. Recent studies have
isolated systematic differences between good quality benthic
records from different regions which have been interpreted as
indicating that the deep Atlantic, which at present is ~2 °C
warmer than the Pacific, was significantly colder than this during
glacial times than at present[5]. However, in these studies it was
only possible to study inter-oceanic gradients; a change in the
average temperature of the whole deep ocean could not be
distinguished from a whole-ocean isotopic change.

We have made a detailed comparison between a deep Pacific
^{18}O record from core V19–30 (ref. 6), and a high-resolution
sea-level record from the Huon Peninsula, New Guinea.
Although neither can be regarded as a perfect monitor of global
ice volume, both records must be dominated by a common
ice-volume signal. In making this comparison, we extend earlier
discussions which noted a discrepancy between sea-level records
of the past 120 kyr as indicated by raised marine terraces, and
by the marine oxygen isotope record[7,8]. The record from core
V19–30 has been fully documented as has the methodology on
which it is based[6]. The Huon sea-level record[9] is less well known
and its derivation is reviewed to clarify the assumptions involved
in comparing it with the ^{18}O record.

Sea-level changes over the past 300 kyr have been interpreted
from a flight of raised coral terraces along the tectonically rising
north-east coast of Huon Peninsula. Individual reef terraces
were dated using the ^{14}C and $^{230}Th/^{234}U$ methods, which have
given good internal consistency within morphological units[10-14].
Each reef developed when the rising sea level overtook the rising
land; reef crests represent approximately the peaks of each
transgression[11,13]. Terrace heights increase southeastwards along
the coast with increasing uplift rates. The morphology and
internal structure of each reef indicates the course of sea-level
change relative to the rising land, so that sea level relative to
stable ocean floor can be extracted for each section if the uplift
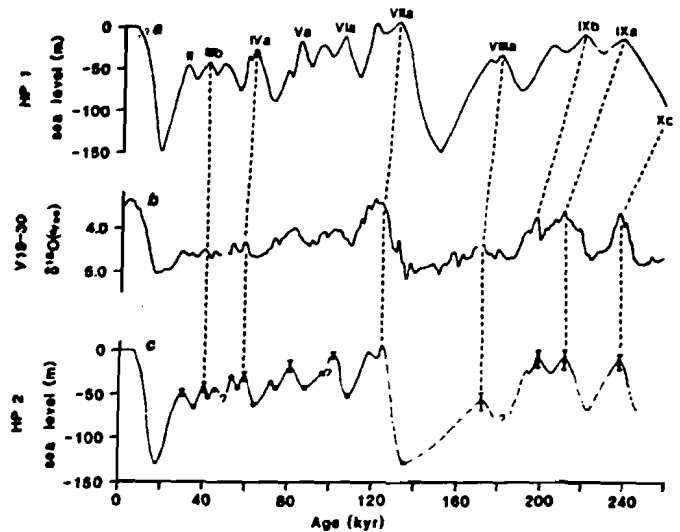rate for that section is known.

Fig. 1 a, Detailed sea-level curve for Huon Peninsula from ref.
9, with small notches eliminated. b, ^{18}O record for the past 340 kyr
from east equatorial core V19–30, from measurements of benthic
Uvigerina senticosa, plotted to an orbitally-tuned timescale and
smoothed with a three-point running mean. c, Detailed sea-level
curve for Huon Peninsula as recalculated after detailed correlation
with the ^{18}O record from core V19–30.

We have estimated uplift rates assuming that sea level at
~125 kyr BP was 6 m above the present level[9-12]. The spread in
radiometric analytical data for this high sea-level event has been
interpreted as indicating that this episode may have been
prolonged. However, stable isotope measurements in both mol-
luscs[15] and corals[16] have confirmed that this interval of high sea
level coincided with the rather short substage 5e in the marine
oxygen isotope sequence. Reef complex VII represents the '125-
kyr marker' in the Huon sequence, and is divided into units
VIIa and VIIb[9-12,17].

Sea levels associated with other Huon reefs were estimated
as follows: given the uplift rate U_j based on the elevation of
reef VII in section j, sea level $S_{i,j} = H_{i,j} - U_j t_i$ where $H_{i,j}$ is the
elevation of the crest of reef i on section j and t_i is the age of
reef i. Sea levels have been estimated for the reef sequence at
seven surveyed sections with uplift rates ranging from
0.9 m kyr^{-1} (north-west end of the flight) to 3.5 m kyr^{-1} (south-
east end of the flight)[12]. Error estimates for the sea level associ-
ated with each reef crest are based on results from all sections,
combined with the contribution of dating errors[9]. The lower sea
levels which intervene between reef crests were estimated in the
same way, using the heights of shallow marine and littoral
deposits in the Tewai section[9], supported by dates from other
sections[13,14].

The detailed sea-level curve for the past 260 kyr derived by
this method is shown in Fig. 1a, modified from the previous
version only in that small steps of a few metres amplitude have
been smoothed out. These steps were interpreted from wave-cut
notches throughout the terrace flight; they seem to represent
individual seismic events and thus have no global validity[9]. The
case for regarding Fig. 1a as a global curve rests on points of
agreement with results from elsewhere. Sea levels at 105, 83 and
60 kyr agree closely with estimates from Barbados[12] and Timor[13]
as well as being supported by dates from the Ryukus[19] and in
Vanuatu (New Hebrides)[20]. Sea level was estimated in these
other areas using the same method, with the reef or terrace of
125 kyr being the reference surface in each case. Agreement
between sites which are widely separated and which have very
different uplift rates supports the global use of the Huon curve.
However, less support is available for the low points, because

Table 1 Heights, uplift rates and sea-level estimates for Huon Terrace sections

Huon Reef	Age (kyr adjusted)	Tewai	Kanzarua	Blucher	Kwambu	Nama	Sambero	Mean sea level
VIIa	124	440	330	280	220	160	150	+6 (assumed)
Uplift (m kyr⁻¹)		3.5	2.61	2.21	1.72	1.24	1.16	(from VIII a)
VIa	100	338*	250	215	160	115	110	
		-12	-11	-6	-12	-9	-6	-9±3
VIb	96	312						
		-24						
Va	81	260	190	155	117	90	80	
		-23	-21	-24	-22	-10	-14	-19±5
Vb	72	216						
		-36						
IVa	59	178	125		70	48		
		-29	-29		-31	-25		-28±3
IVb†	53	156						
		-30						
IIIa	45	112						
		-46						
IIIb	40	98	70	41	28	10		
		-42	-34	-47	-41	-40		-41±4
II	28	52	30	18	7			
		-46	-43	-44	-41			-44±2

Height data are from ref. 9 (Tewai) and ref. 12 (other sections). Heights of reef VIIa at all except Tewai and Kwambu are as given for VIIb in ref. 12. Uplift rate is based on VIIa = 12 kyr, sea level at +6 m.

* Estimated, not surveyed, height. All other heights are from theodolite survey.

† Heights of IVb and IIIa based only on Tewai section, as uncertainty exists over whether IIIa surveyed on other sections is equivalent to 53- or 45-kyr isotope points.

the low sea-level deposits are generally buried by those of the subsequent transgression. Low sea-level points are a good test of the global applicability of the curve because isostatic and other factors will probably have their greatest effect between glacial maxima and minima.

The low sea level at 18 kyr corresponding to the last glacial maximum is an important point for comparison with ^{18}O records. Figure 1a shows this level at −150 m based mainly on results from northern Australia where lagoonal facies at −135 m (ref. 21), intertidal beach rock at −150 m (ref. 22), and coral below a terrace at −165 m (ref. 23) occur at sites on the outer shelf margins and are dated between 14 and 18 kyr. Lesser values, around −90 to −110 m are reported from the west Atlantic[24] and Texas Gulf[25]. Variations around the globe are to be expected as a result of adjustment to glacial/interglacial changes of ice and ocean volumes[26-28], although the magnitude of predicted variation differs from one geophysical model to another. The sea-level change between 18 kyr and the present on a broad shelf would be expected to be larger than that recorded on a dipstick-type margin such as the Huon Peninsula[28-30], so that 150 m may be an overestimate of the 18-kyr level at Huon. Undated evidence does occur at Huon in the form of a submerged terrace running along the submarine margin. This is narrow and coraline where it occurs in front of coral terraces, and broad and gravelly where it lies off the flank of a broad deltaic plain[11]. Correcting its level for local uplift puts the sea level at −130 m for each locality[11]. In view of this consistency, we use this estimate of −130 m in our subsequent discussion.

The δ^{18}O record from core V19-30, based on Uvigerina senticosa, is shown in Fig. 1b. The original sampling interval of 3 cm corresponds to ~500 yr on average although this value varies down the core as accumulation rate varies[6,31]. Figure 1b shows the record using a timescale that was developed by the SPECMAP project[32], and smoothed using a three-point running mean. This timescale was developed iteratively, the starting point being radiometric age determinations both in marine sediments and in coral terraces. The final timescale is developed by tuning the initial record on the basis of its relationship to orbital precession, obliquity and eccentricity functions[32,33]. Although

the final timescale is not dependent in detail on particular radiometric dates, the modifications are within the uncertainties of the age estimates at all points[32,33]. In fact, the orbital theory does not provide sufficient constraints on the timescale within stage 3 (in the range 30–60 kyr BP) so that no significant departures from the chronology implied by direct radiometric dating have been used in this interval.

We consider that for the part of the record older than stage 3, the orbitally tuned timescale should be used to refine the age estimates for the Huon Peninsula reefs, on the grounds that independent lines of evidence converge in support of this mechanism, and that the assumption of orbital forcing places constraints on the timescale from 70 kyr back past the useful limits of U-series dating that are much tighter than those imposed by the analytical uncertainties on radiometric dates in this interval. Figure 1c shows the Huon sea-level record as re-estimated on this basis; each sea-level maximum and minimum has been assigned the same age as the assumed correlative in the V19-30 record. The amplitude of some peaks differs significantly between Fig. 1a and c because the sea-level estimate for any point in the sequence depends on the assumed age for that point. The sea level also depends on the value of the uplift rate adopted in each section which depends on the age assumed for reef VII. It also depends on whether this age, and the 6-m calibration height, is assigned to terrace VIIa or VIIb. Finally in traverses containing a single feature for reef VII the uplift rate depends on whether this feature is assumed to represent VIIa or VIIb. Because oxygen isotope studies clearly associate reef VIIa (the older) with substage 5e (ref. 17), and also associate the undifferentiated but dated level in Barbados[15,16] and in Curacao with 5e, it must be assumed that VIIa is the calibration level to make a comparison consistent with the deep-sea ^{18}O record. There are various sources of data from the Huon Peninsula[9-14], so to remove confusion, Table I lists reef crest heights from each surveyed traverse together with the age that we have adopted for each, and the resulting sea-level estimate.

Before 130 kyr the sea-level curve derived from marine terraces is subject to larger uncertainties because both the assigned ages and assumed uplift rates become less secure. However, for
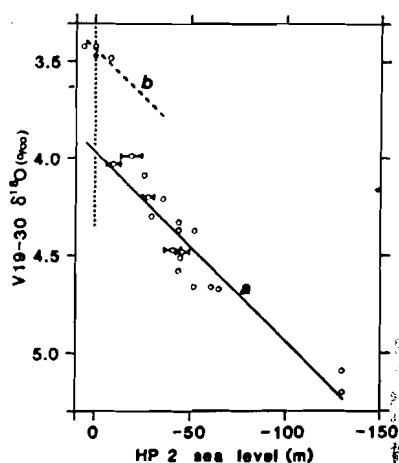
Fig. 2 Huon sea level (recalculated age model, Fig. 1c) versus equivalent [18]O in V19-30, from data in Table 2. Regression line a, $\delta^{18}O = 3.96-0.0097$ sea level, fitted to all points from 17 to 112 kyr, $r^2 = 0.86$. Line b is drawn parallel to the regression line a, but passes the area at top left which encompasses data for 5e (124 kyr) and recent (6 kyr-present).

Table 2 Huon sea levels and V19-30 [18]O values

Huon Reef	Age HP1 (kyr)	Sea level HP1 (m)	Age HP2 (kyr)	Sea level HP2 (m)	$\delta^{18}O$
Modern	0	0	0	0	3.42
I	6	0	6	0	3.47
I/II	18	−150	17	−130	5.09
II	30	−46	29	−46	4.48
II/IIIb	34	−62	35	−65	4.67
IIIb	40	−40	40	−41	4.47
IIIb/a	43	−57	42	−52	4.66
IIIa	47	−42	44	−45	4.51
IIIa/IVb	55	−78	?	?	—
IVb	58	−36	53	−30	4.30
IVb/a	60	−40	56	−44	4.58
IVa	62	−27	59	−28	4.20
IVa/Vb	72	−88	64	−61	4.66
Vb	77	−52	72	−36	4.21
Vb/a	79	−60	74	−44	4.33
Va	83	−18	81	−19	3.99
Va/VIb	89	−48	88	−44	4.37
VIb	95	−22	96	−26	4.09
VIb/a	99	−38			
VIa	105	−12	106	−19	4.03
VIa/VIIb	112	−60	112	−62	4.38
VIIb	120	+4	118	0	3.49
VIIb/a	123	−8	122	−8	—
VIIa	132	+6	124	+6	3.37
VII/VIII	150	−145	135	−130	5.20

the past 130 kyr we regard Fig. 1c as the best sea-level record available for the New Guinea/Australian region (noting that the magnitude of sea-level oscillations may be smaller in other parts of the world as a result of isostatic factors). Within the past 130 kyr the greatest uncertainty relates to the reef IVb-IIIa area where the isotopic record shows little structure (see Table 2); in Fig. 1c a gap is shown over this part. Table 2 lists sea levels for most turning points in Fig. 1a,c as well as the [18]O values for corresponding points in V19-30.

Comparing Fig. 1b with Fig. 1c, it is particularly striking that the sea-level peaks within the last glacial cycle, and especially the well controlled peaks at ~106 and 81 kyr, are relatively closer to the Recent and 124-kyr levels than the equivalent [18]O values. Figure 2 plots sea level against [18]O for all established turning points in Fig. 1c. A cluster of points around zero sea level and +3.4‰ corresponds to full interglacial stage 1 and substage 5e. A single line cannot be drawn through all data points: that is, there is not a simple linear relationship between sea level and [18]O in benthic foraminifera. Although this situation could result in part from temporal variations in the isotopic composition of the stored ice, this cannot be the chief factor involved. If the 0.6‰ isotopic difference between the interglacial points and the two terraces at ~−20 m were to be explained solely in terms of the removal of isotopically light water from the ocean, this would necessitate ice with an [18]O content of ~100‰. The lightest ice in Antarctica is ~−60‰[34,35]. The average isotopic composition of the ice in an ice sheet depends mainly on the isotopic composition of the snow falling in the cold central region, which depends on the air temperature and hence mainly on the altitude of the central part. Thus the first ice accumulating in small Northern hemisphere ice sheets must have been less isotopically light than was the ice stored in the fully developed ice sheet.

One possible solution to this difficulty could be that a significant amount of isotopically light floating ice accumulated[36-38]. This would change the ocean isotopic composition without having any effect on sea level. The only place where a sufficient quantity of floating ice can plausibly be envisaged is the Arctic Ocean; the detailed and continuous stratigraphic sequences that have recently been documented from deep-sea cores in the Eastern Arctic Basin[39] exclude the possibility that this ingenious idea is correct, at least for the 18 kyr glacial maximum. The data in Fig. 2 require a mechanism that operated during warm substages 5a and 5c as well as at glacial maximum time.

A more probable explanation is that this isotopic shift results

from a temperature effect on the isotopic composition of the benthic foraminifera analysed. A best-fit line through all the glacial points in Fig. 2 intercepts the axis at ~+3.95‰ (line a on Fig. 2), requiring a temperature difference of ~2 °C. The slope of this line is 0.97‰ per 10 m (very close to the generally adopted value[40]) which corresponds to a mean [18]O content for the abstracted water of ~−35‰, a reasonable value.

Deviations from this regression are still significant; in Fig. 3 we examine the temporal pattern of the deviations from line b on Fig. 2, which parallels line a and passes the Recent points, to evaluate the relative contributions of varying sea level, deep-water temperature and ice isotopic composition to the [18]O record. For convenience, Fig. 3 has a scale representing deep-water potential temperature at the site of core V19-30 (refs 41, 42). This scale would be valid only if there were no variation in the isotopic composition of stored ice-sheet ice. If this assumption is correct, Pacific deep waters cooled rapidly to ~0 °C by ~110 kyr, and then cooled more slowly to ~−1 °C around 40 kyr, warming to 0 °C at 18 kyr and then to 1.5 °C at present. Although a warming at 18 kyr seems surprising, one model has predicted such an effect[43]. However, an alternative would be that the stored ice (which includes Antarctic ice) became gradually more negative between 110 and 30 kyr (ref. 44), and that the very rapid advance of ice to lower latitudes between 30 and 20 kyr involved more temperate ice that was less isotopically negative. Further work will be needed to establish the possible contribution of temperature variability to the pattern in the glacial section of Fig. 3; we regard the overall glacial cooling of Pacific deep water by 1.5 °C that is implied, as inescapable.

It would be useful to compare the older sections of the Huon and V19-30 records, but this is not possible for several reasons: (1) there is no earlier sea-level datum comparable to that at 124 kyr to use for uplift-rate calibration; (2) the errors in [230]Th/[234]U dates become more serious in this interval; Fig. 1 suggests that this method may actually overestimate ages in the 180-240 kyr age range; (3) only two sections have been surveyed for the pre-5e part of the Huon record. It is regrettable that the morphostratigraphy of this important Upper Quaternary area has been surveyed and described by only one geologist (J.C.).
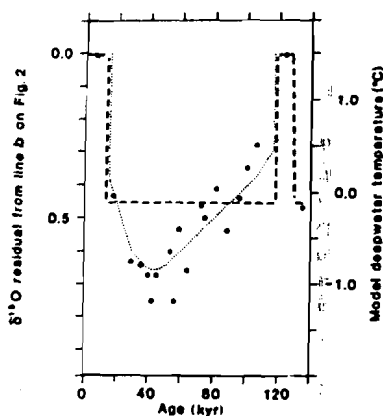
Fig. 3 Residuals from line *b* (Fig. 2) versus estimated age. Scale to right shows calculated potential temperature at the sea floor at the site of core V19-30, if this line is interpreted as the correct relationship between sea level and ocean $\delta^{18}O$, and deviations from the line ascribed to temperature. Heavy dashed line is our preferred interpretation of the temperature record; the light dotted line is an alternative.

No other area is known where the details of sea-level change are available for field examination.

We conclude that deep waters in the Pacific Ocean were ~1.5 °C cooler in glacial and interstadial times than in the short (~10 kyr duration) interglacials of substage 5e and the present. One interpretation of our analysis is that deep water was coldest at ~40 kyr and that almost 1 °C of warming occurred by the glacial maximum and a further 1.5 °C of warming subsequently. Alternatively, part of the observed detail resulted from changes in the isotopic composition of the ice sheets, with the deep Pacific remaining ~1.5 °C cooler than the present temperature throughout the glacial. Regardless of this detail, massive cooling of the already cold abyssal ocean must be considered an important aspect of the ice age climate.

This work was supported in Cambridge by the NERC. N.J.S. acknowledges stimulating discussion with many colleagues, particularly J.-C. Duplessy.

1. Emiliani, C. J. Geol. 63, 538-538 (1955).
2. Epstein, S., Buchsbaum, R., Lowenstam, H. A. & Urey, H. C. Bull. geol. Soc. Am. 62, 417 (1951).
3. Epstein, S. & Mayeda, T. Geochim. cosmochim. Acta. 4, 213-224 (1953).
4. Berger, W. H., Killingley, J. S. & Vincent, E. Oceanol. Acta 1, 221-230 (1978).
5. Duplessy, J.-C., Moyes, J. & Pujol, C. Nature 286, 479-481 (1980).
6. Shackleton, N. J., Imbrie, J. & Hall, M. A. Earth planet. Sci. Lett. 65, 233-244 (1983).
7. Broecker, W. S. Science 188, 1116-1121 (1975).
8. Dodge, R. E., Fairbanks, R. G., Benniger, L. K. & Maurrasse, F. Science 219, 1423-1424 (1983).
9. Chappell, J. Search 14, 99-101 (1983).
10. Veeh, H. H. & Chappell, J. Science 167, 862-865 (1970).
11. Chappell, J. Bull. geol. Soc. Am. 85, 553-570 (1974).
12. Bloom, A. L., Broecker, W. S., Chappell, J., Matthews, R. K. & Mesolella, K. J. Quat. Res. 4, 185-205 (1974).
13. Chappell, J. & Polach, H. A. Bull. geol. Soc. Am. 87, 235-240 (1976).
14. Chappell, J. & Veeh, H. H. Nature 276, 602-603 (1978).
15. Shackleton, N. J. & Matthews, R. K. Nature 268, 618-620 (1977).
16. Fairbanks, R. G. & Matthews, R. K. Quat. Res. 10, 181-196 (1978).
17. Aharon, P., Chappell, J. & Compston, W. Nature 283, 649-651 (1980).
18. Chappell, J. & Veeh, H. H. Bull. geol. Soc. Am. 89, 356-368 (1978).
19. Kohishi, K., Omura, A. & Nakamichi, O. Proc. 2nd int. Coral Reef Symp. 2, 595-613 (1973).
20. Neef, G. & Veeh, H. H. Nature 269, 682-683 (1977).
21. Van Andel, Tj. & Veevers, J. J. Bur. Miner. Res., Aust. Bull. 3 (1967).
22. Jongsma, D. Nature 228, 150-151 (1970).
23. Veeh, H. H. & Veevers, J. J. Nature 226, 536-537 (1970).
24. Milliman, J. D. & Emery, K. O. Science 162, 1121-1122 (1970).
25. Curray, J. Recent Sediments, Northwest Gulf of Mexico (ed. Sheppard, F. P.) 221-266 (American Association of Petroleum Geologists, Tulsa, 1960).
26. Walcott, R. I., Quat. Res. 2, 1-14 (1970).
27. Cathles, L. M. in Earth Rheology, Isostasy and Eustasy (ed. Morner, N. A.) 11-44 (Wiley, New York, 1980).
28. Clark, J. A., Farrell, W. E. & Peltier, W. R. Quat. Res. 9, 265-287 (1978).
29. Bloom, A. L. Bull. geol. Soc. Am. 78, 1477-1494 (1967).
30. Chappell, J. Quat. Res. 4, 405-428 (1974).
31. Shackleton, N. J. & Pisias, N. G. in Atmospheric CO₂: Natural Variations, Archaean to Present (eds Sundquist, E. T. & Broecker, W. S.) 303-317, Am. geophys. Un. monogr. 32 (1985).
32. Imbrie, J. et al. in Milankovitch and Climate (eds Berger, A. et al.) 269-305, (Reidel, Dordrecht 1984).
33. Hays, J. D., Imbrie, J. & Shackleton, N. J. Science 194, 1121-1132 (1976).
34. Dansgaard, W., Johnson, S. J., Moller, J. & Langway, C. C. Science 166, 377-381 (1969).
35. Picciotto, E., Cameron, R., Crozaz, G., Deutsch, S. & Wilgain, S. J. Glaciol. 7, 273-287 (1968).
36. Mercer, J. H. Palaeogeogr., Palaeoclimatol. Palaeoecol. 8, 19-27 (1970).
37. Broecker, W. S. Science 188, 1116 (1975).
38. Williams, D. F., Moore, W. S. & Fillon, R. H. Earth planet. Sci. Lett. 56, 157-166 (1981).
39. Markussen, B., Zahn, R. & Thiede, J. Palaeogeogr. Palaeoclimatol., Palaeoecol. 50, 271-284 (1985).
40. Shackleton, N. J. & Opdyke, N. D. Quat. Res. 3, 39-55 (1973).
41. O'Neil, J. R., Clayton, R. N. & Mayeda, T. K. J. chem. Phys. 51, 5547-5558 (1969).
42. Shackleton, N. J. Colloq. Int. cent. Nat. Res. Scient. 219 (1974).
43. Newell, R. Quat. Res. 4, 117-126 (1974).
44. Mix, A. C. & Ruddiman, W. F. Quat. Res. 21, 1-20 (1984).

Predicting aqueous aluminium concentrations in natural waters

Christopher S. Cronan, William J. Walker* & Paul R. Bloom†

Department of Botany and Plant Pathology, University of Maine, Orono, Maine 04469, USA
* Land and Water Resources Center, University of Maine, Orono, Maine 04469, USA
† Department of Soil Science, University of Minnesota, St. Paul, Minnesota 55108, USA

Aluminium is a pH-sensitive element that can cause acute toxicity symptoms in some organisms at aqueous activities of 10 μM or less[1-3]. Scientists working on agricultural systems have long been concerned with the deleterious effects of aluminium on crop roots[4,5]. More recently, environmental scientists have reported a potentially harmful biogeochemical link between acidic deposition onto forest soils and aluminium toxicity in forest and aquatic communities of northeastern North America and northern Europe[6-8]. Because of this general interest in aluminium toxicity as an environmental threat, there have been renewed efforts to model the chemistry and transport of aqueous aluminium in soils and surface waters. Here we propose that much of the spatial and temporal variability in aqueous aluminium chemistry can be accounted for by a two-component equilibrium model involving a solid-phase humic adsorbent and an aluminium trihydroxide mineral phase. Inputs for the model are solution pH, copper-extractable organic aluminium and the titratable carboxyl content of soil humus.

Several workers[9,10] have found that $[Al^{3+}]$ (aquo aluminium ion activity) in surface waters can be predicted accurately as a function of pH using an aluminium trihydroxide solubility relationship. However, other reports[11-13] have presented data revealing aluminium concentrations that are much lower than predicted—that is, despite pH values less than 4.5 and elevated concentrations of complexing organic ligands, the solutions contained low concentrations of soluble aluminium. This illustrates the failure of existing geochemical models to account for all the major variations in $[Al^{3+}]$ and we refer to it as the 'paradox of aluminium undersaturation'.

Figure 1 shows $[Al^{3+}]$ for a variety of natural waters from North America and northern Europe. The expected pAl^{3+} values for solutions in equilibrium with natural gibbsite and amorphous $Al(OH)_3$ are also shown. As illustrated, there are three major points where observed and predicted aqueous aluminium activities diverge: the upper soil rooting zone, downstream of wetlands and during stream peak flows. While it has been suggested that these cases of lowered $[Al^{3+}]$ are the result of kinetic constraints on the dissolution of mineral aluminium[14], there have been no rigorous efforts to confirm the kinetic hypothesis in natural systems. In this study, our objective was to derive a model that could account for these 'undersaturated'